

# Stiffening of matter in quark-hadron continuity

Toru Kojo<sup>1</sup>

<sup>1</sup>*Key Laboratory of Quark and Lepton Physics (MOE) and Institute of Particle Physics,  
Central China Normal University, Wuhan 430079, China*

(Dated: April 14, 2022)

We discuss stiffening of matter in quark-hadron continuity. We introduce a model that relates quark wavefunctions in a baryon and the occupation probability of states for baryons and quarks in dense matter. In dilute regime, the confined quarks contribute to the energy density through the masses of baryons, but do not directly contribute to the pressure, hence the equations of state are very soft. This dilute regime continues until the low momentum states for quarks get saturated; this may happen even before baryons fully overlap, possibly at density slightly above the nuclear saturation density. After the saturation the pressure grows rapidly while changes in energy density are modest, producing a peak in the speed of sound. If we use baryonic descriptions for quark distributions near the Fermi surface, we reach a description similar to the quarkyonic matter model of McLerran and Reddy. With a simple adjustment of quark interactions to get the nucleon mass, our model becomes consistent with the constraints from 1.4-solar mass neutron stars, but the high density part is too soft to account for two-solar mass neutron stars. We delineate the relation between the saturation effects and short range interactions of quarks, suggesting interactions that leave low density equations of state unchanged but stiffen the high density part.

## I. INTRODUCTION

How highly compressed baryonic matter transforms into quark matter has been a long standing question in Quantum Chromo Dynamics (QCD) [1, 2]. Considering the size of a baryon of 0.5 – 0.8 fm, we expect the transition to take place at  $n_B = 2 - 10n_0$  ( $n_0 \simeq 0.16 \text{ fm}^{-3}$ : nuclear saturation density). The difficulties to describe the transition lie in treatments of nonperturbative effects such as confinement, chiral restoration, or other strong correlation effects [3–5]. The lattice Monte Carlo simulations suitable for strong coupling regimes are not usable at finite density, while perturbative calculations based on the weak coupling picture are not applicable at  $n_B \lesssim 40n_0$  [6–14]. The framework based on low energy nuclear physics [15–22] is reliable only to  $n_B = 1.5 - 2n_0$  beyond which we must perform some extrapolation toward high density.

In spite of all these difficulties, the combined use of the above information and recent neutron star (NS) observations [23–29] allows us to get insights on the properties of dense matter (see, e.g., [30] for a short review). Recent analyses by NICER, including the radius measurements of  $2.08M_\odot$  ( $M_\odot$ : solar-mass) and  $1.4M_\odot$  NSs, constraints from the NS merger event GW170817, and nuclear physics constraints, yielded the estimates of the radii  $R_{2.08} \simeq R_{1.4} \simeq 12.4 \text{ km}$  [31, 32]. This small variation in the radii from  $1.4M_\odot$  to  $2.08M_\odot$  NS suggests that the equation of state (EoS) for  $n_B = 2 - 5n_0$  should not contain substantial softening, but rather should get stiffened. This feature disfavors strong first order phase transitions in the domain  $n_B = 2 - 5n_0$ , although the weaker one is still possible.

Since the first discovery of  $2M_\odot$  NS [25], a number of works have been devoted to the crossover description for hadron-to-quark phase transitions [33–40]. Early works [33–35] phenomenologically interpolated hadronic EoS at

$n_B \lesssim 2n_0$  and quark matter EoS at  $n_B \gtrsim 4n_0$ ; the resulting EoS is consistent with the existing NS constraints, and has a novel peak structure in the speed of sound  $c_s = (\partial\mathcal{P}/\partial\varepsilon)^{1/2}$  where  $\mathcal{P}$  and  $\varepsilon$  are pressure and energy density, respectively. Later, such a peak structure was discussed as generic, by noting the contrast between stiffness of low and high density EoS [41]; nuclear physics calculations suggest soft low density EoS which must get stiffened rapidly to pass the  $2M_\odot$  mass constraints [42, 43]. This peak should have a mechanism specific to dense matter [44, 45]; in the finite temperature crossover from a hadron resonance gas to a quark-gluon plasma, the speed of sound has a dip, instead of a peak, as one can see from the lattice simulations [46].

The microscopic mechanism for the emergence of the peak has been discussed by McLerran and Reddy (MR) [47], who used the concepts of quarkyonic matter [48]. The quarkyonic matter is a quark matter with a baryonic Fermi surface, and the excitations are confined [49–58]. In the MR model, they used a hybrid description in momentum space; a matter at low density is dominated by baryons, but as density increases, the quark Fermi sea emerges at low momenta, pushing up the baryonic states to high momenta. For suitable choices of parameters, baryons become relativistic at  $n_B = 1.5 - 3n_0$  with a substantial peak in  $c_s$ . The advantage of the MR model is that relativistic baryons emerge by the quark Pauli blocking mechanism which is independent of details in nuclear forces, and hence the mechanism is qualitatively robust. Several successful descriptions of the NS have originated from this framework [59–66].

In this paper we discuss the stiffening of dense matter associated with the *saturation* of quark states at low momenta that may be regarded as the onset of the quark Fermi sea. The preliminary discussion was given in Ref.[67], and this paper is the fuller version. This work is basically a follow-up work of Ref.[47], but con-

tains new attempts and insights which can be potentially important:

Firstly, we describe the crossover behavior using quark degrees of freedom only, starting with the description of a single baryon, proceeding to a baryonic matter, and to a quark matter formation. Although the descriptions are rather crude, this approach has the advantage over conventional hybrid descriptions where one use quarks in one place and baryons (hadrons) in the other place. This removes the worries about double counting as well as the confusions associated with switching in degrees of freedom<sup>1</sup>. The onset density of quark matter formation is related to the size scale of a baryon, and we found that the saturation begins to occur slightly above the nuclear regime,  $1 - 3n_0$ , even before baryon cores overlap. The softness in baryonic matter and stiffness in quark matter are described in a unified manner. We also check how our quark descriptions are related to the MR model.

Secondly, we attempt to describe in-medium interactions at the level of quark descriptions. This is potentially important, considering the difficulties to predict two-, three-, and more-body baryonic forces at high density. It has been known that a simple constituent quark model with one-gluon-exchanges accounts for the baryon spectroscopy remarkably well [70, 71]. Recent lattice calculations for baryon-baryon interactions even show that the simple constituent quark picture correctly describes the observed patterns of baryon-baryon interactions, including the hard core repulsion among nucleons as well as baryon interactions with strangeness [72–74]. These successes in describing semi-short range correlations, at momentum scale  $\sim 0.2 - 1$  GeV, give us a hope to build a unified description for the properties of matter from the baryonic to quark matter regime. In this spirit, relevant interactions at  $\sim 5 - 10n_0$ , at lower density than for the perturbative regime, have been examined [36–38, 75, 76]. The present framework solely based on quarks is suitable for the unified treatments of interactions.

In Sec.II we begin with quarks in a baryon, and in Sec.III discuss quarks in a baryonic matter. In Sec.IV quark matter formation and the associated stiffening are described. In Sec.V we mention how our descriptions are related to the MR model. In Sec.VI we discuss the spin-flavor quantum numbers of baryons and how they fill the quark spin-flavor states. In Sec.VII we discuss interactions for matter from dilute baryonic to dense quark regime, and examine what kind of interactions is suitable to describe the NS phenomenology. Sec.VIII is devoted for summary.

<sup>1</sup> The double counting introduces serious problems into field theoretic computations for the zero point energy in matter [68]. The UV divergences appear from both elementary and composite particles. Consistent treatments of both contributions are mandatory to cancel the divergences in medium by the vacuum subtraction of the energy [69].

## II. QUARKS IN A BARYON

We consider how quark states are occupied as baryon density increases. We postulate a distribution of quarks with the momentum  $\mathbf{p}$  which belong to a baryon with the momentum  $\mathbf{P}_B$ ; the form is given by

$$Q_{\text{in}}(\mathbf{p}, \mathbf{P}_B) = \mathcal{N} e^{-\frac{1}{\Lambda^2} \left( \mathbf{p} - \frac{\mathbf{P}_B}{N_c} \right)^2}, \quad (1)$$

where  $\Lambda$  is the scale of the order of the QCD nonperturbative scale,  $\Lambda_{\text{QCD}} \simeq 0.2 - 0.3$  GeV, related to the radius of a baryon as  $\Lambda \sim R_{\text{baryon}}^{-1}$ , and  $\mathcal{N}$  is the normalization constant

$$\mathcal{N} = \frac{8\pi^{3/2}}{\Lambda^3}, \quad (2)$$

with which  $\int_{\mathbf{p}} Q_{\text{in}} = 1$ . The momentum distribution becomes broader for a smaller baryon radius.

The sum of  $N_c$  quark momenta ( $N_c$ : number of colors) should be  $\mathbf{P}_B$ , and the distribution satisfies this condition at the level of the expectation value,

$$\langle \mathbf{P}_B \rangle = N_c \int_{\mathbf{p}} \mathbf{p} Q_{\text{in}}(\mathbf{p}, \mathbf{P}_B). \quad (3)$$

More realistically the probability distribution of a quark must be related to those of the other  $N_c - 1$  quarks, but in this paper we consider only the averaged description for quark momentum distributions.

As the quark momentum has the broad distribution, the magnitude of momentum is substantial,

$$\left\langle \left( \mathbf{p} - \frac{\mathbf{P}_B}{N_c} \right)^2 \right\rangle \sim \Lambda^2. \quad (4)$$

independent of  $\mathbf{P}_B$ , and hence quarks can be energetic compared to the baryon kinetic energy or the nuclear scale of  $O(1 - 10)$  MeV. This disparity will be reflected in the large energy density but small pressure in baryonic matter.

Below we approximate the baryon energy as the sum of the energies from  $N_c$  quarks. The energy of a quark in a baryon with momentum  $\mathbf{P}_B$  is

$$\begin{aligned} \langle E_q(\mathbf{p}) \rangle_{\mathbf{P}_B} &= \left\langle E_q \left( \mathbf{p} + \frac{\mathbf{P}_B}{N_c} \right) \right\rangle_{\mathbf{P}_B=0} \\ &\simeq \langle E_q(\mathbf{p}) \rangle_{\mathbf{P}_B=0} + \frac{1}{2} \left\langle \frac{\partial E_q}{\partial \mathbf{p}^2} \right\rangle_{\mathbf{P}_B=0} \left( \frac{\mathbf{P}_B}{N_c} \right)^2 + \dots, \end{aligned} \quad (5)$$

where the term linear in  $\mathbf{P}_B$  vanishes. It is important to note that the correction from finite  $\mathbf{P}_B$  is suppressed by  $1/N_c^2 \sim 1/10$ , and the quark single particle energy is hardly affected by the baryon momentum until  $P_B$  becomes very large,  $\sim N_c \Lambda$ .

The simplest version of our model includes only a potential localizing quarks, and the resulting baryon energy is simply

$$E_B \simeq N_c \langle E_q(\mathbf{p}) \rangle_{\mathbf{P}_B}. \quad (6)$$

For instance, in a non-relativistic quark model

$$E_B^{\text{NRq}} = N_c \left( M_q + \frac{\Lambda^2}{2M_q} \right) + \frac{\mathbf{P}_B^2}{2N_c M_q} + \dots, \quad (7)$$

and the kinetic energy of the baryon is suppressed by the large baryon mass,  $M_B \equiv E_B(P_B = 0)$ .

It is important to note that  $M_B$  in our model is considerably larger than  $N_c M_q$  by the kinetic energy  $\sim \Lambda$  of each quark. If we use usual constituent quark mass of  $M_q \sim 0.3$  GeV for up- and down-quarks, there must be attraction of  $\sim \Lambda$  to keep the picture of  $M_B \sim N_c M_q$ . In Sec. VII we will consider such short range interactions to modify the average single particle energy and to get the right baryon mass.

### III. QUARKS IN BARYONIC MATTER

#### A. Occupation probability of quark states

The occupation probability of quark states,  $f_q(p; n_B)$ , increases as the baryon number does, and also depends on the occupation probability of baryon states,  $\mathcal{B}(P_B; n_B)$ . Below we assume that the probability depends only on the size of momenta,  $p = |\mathbf{p}|$  and  $P_B = |\mathbf{P}_B|$ . With a quark distribution in a baryon, the probabilities  $f_q$  and  $\mathcal{B}$  are related as

$$f_q(p; n_B) = \int_{\mathbf{P}_B} \mathcal{B}(P_B; n_B) Q_{\text{in}}(\mathbf{p}, \mathbf{P}_B). \quad (8)$$

That is, we sum up the quark occupation probability from each baryonic states.

In dilute regime, we can neglect interactions among baryons as they are widely separated in space. Baryons fill the states from low momenta with the probability 1, as in an ideal gas; ( $N_f$ : number of flavors)

$$\mathcal{B}(P_B; n_B) = \theta(P_F - P_B), \quad n_B = N_f \frac{P_F^3}{3\pi^2}, \quad (9)$$

where  $P_F$  is the Fermi momentum of baryons.

Let us look at how  $f_q$  evolves as  $n_B$  increases. In the following we rescale momenta

$$\tilde{p} = p/\Lambda, \quad \tilde{P}_B = P_B/N_c\Lambda, \quad \tilde{P}_F = P_F/N_c\Lambda, \quad (10)$$

with which  $f_q$  can be written as

$$f_q(p; n_B) = \mathcal{N} \frac{(N_c\Lambda)^3}{(2\pi)^2} \int_0^{\tilde{P}_F} \tilde{P}_B^2 d\tilde{P}_B e^{-(\tilde{p}^2 + \tilde{P}_B^2)} \times \int_{-1}^1 d\cos\theta e^{2\tilde{p}\tilde{P}_B \cos\theta}. \quad (11)$$

We note that, in dilute regime,  $\tilde{P}_F \ll 1$  or  $P_F \ll N_c\Lambda$  so that the domain for the integral over  $\tilde{P}_B$  is very small, cancelling the overall factor  $(N_c\Lambda)^3$ . As  $\tilde{P}_B$  in the exponent of the integrand can be regarded as small, we expand them and find

$$f_q \simeq \mathcal{N} \frac{P_F^3}{6\pi^2} e^{-\tilde{p}^2} \left( 1 + \frac{-3 + 2\tilde{p}^2}{5} \tilde{P}_F^2 + \dots \right). \quad (12)$$

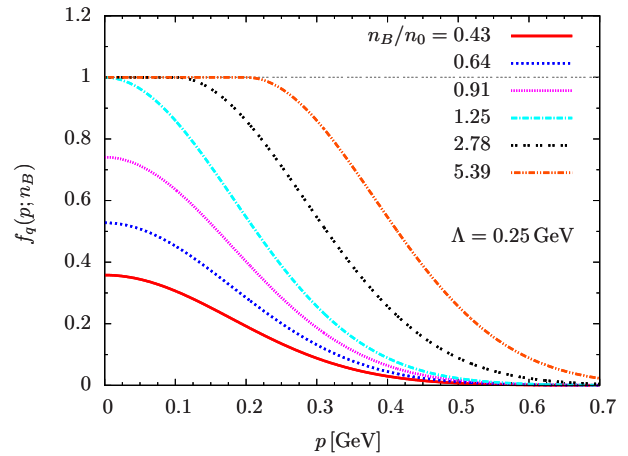


FIG. 1. The quark occupation probability  $f_q(p; n_B)$ , for various  $n_B/n_0$ . We took  $\Lambda = 0.25$  GeV and  $N_c = 3$ .

Recalling  $\mathcal{N} \sim \Lambda^{-3}$ , the overall size of  $f_q$  is  $\sim (P_F/\Lambda)^3$ . As for the shape, the leading order contribution maintains the Gaussian form. Some examples are shown in Fig. 1. Here  $f_q$  for various  $n_B/n_0$  are shown for  $\Lambda = 0.25$  GeV and  $N_c = 3$ . The curves up to  $n_B/n_0 = 1.25$  are compatible with the quark Pauli blocking. Remarkably, the shape of  $f_q$  hardly changes, while the size grows linearly in  $n_B$ .

In the large  $N_c$  limit, one can derive a number of simple expressions as we may neglect  $\tilde{P}_F$  terms 12. The  $f_q$  takes the form

$$f_q(p; n_B)|_{N_c \rightarrow \infty} = \mathcal{N} \frac{P_F^3}{6\pi^2} e^{-\tilde{p}^2} = \frac{n_B}{n_B^c} e^{-\tilde{p}^2}. \quad (13)$$

where the  $p = 0$  state gives the largest  $f_q$ , and is saturated at  $n_B^c = N_f (P_F^c)^3 / 3\pi^2$ ; the corresponding baryon Fermi momentum is

$$1 = f(0; P_F^c) \leftrightarrow P_F^c|_{N_c \rightarrow \infty} = \Lambda \left( \frac{3\sqrt{\pi}}{4} \right)^{1/3} \simeq 1.1\Lambda. \quad (14)$$

Actually this estimate based on the large  $N_c$  turns out to be a reasonable approximation to the  $N_c = 3$  result.

In Fig. 2 the  $f_q(p = 0; n_B)$  is shown as a function of  $n_B$  for  $N_c = 3$ . For a larger  $\Lambda$  the baryon radius is smaller and the saturation of the  $p = 0$  state happens at larger  $n_B$ . It is important to note that, for  $\Lambda = 0.2 - 0.3$  MeV as the reasonable scale of baryon radii, the saturation takes place at  $n_B = 0.5 - 2n_0$ ; this baryon density is within or close to the territory of conventional nuclear physics. The reason why this may happen before the baryon cores overlap is that wavefunctions have broader extension than the average baryon size.

#### B. Equations of state in dilute baryonic matter

Next we compute the EoS using the occupation probability discussed in the previous section. For simplicity

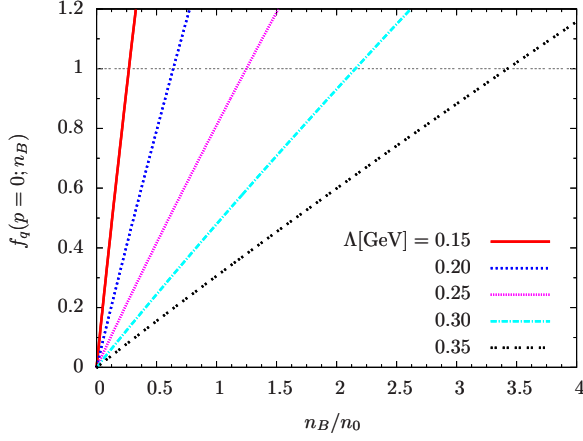


FIG. 2. The  $n_B$  dependence of the quark occupation probability at zero momentum,  $f_q(p=0; n_B)$ , for  $\Lambda = 0.15, 0.20, 0.25, 0.30$ , and  $0.35$  GeV. We took  $N_c = 3$ . The growth in  $f_q(p=0; n_B)$  is almost linear in  $n_B$ .

we assume the quark energy of the form

$$E_q(p) = \sqrt{p^2 + M_q^2}. \quad (15)$$

The energy density is computed as

$$\varepsilon(n_B) = 2N_c N_f \int_{\mathbf{p}} E_q(p) f_q(p; n_B). \quad (16)$$

The chemical potential is computed as

$$\mu_B = \frac{\partial \varepsilon}{\partial n_B} = 2N_c N_f \int_{\mathbf{p}} E_q(p) \frac{\partial f_q(p; n_B)}{\partial n_B}. \quad (17)$$

The expression is particularly simple in the large  $N_c$  limit; using Eq.(13), we find

$$\varepsilon^{N_c \rightarrow \infty} = n_B N_c \mathcal{N} \int_{\mathbf{p}} E_q(p) e^{-\tilde{p}^2} = n_B M_B^{N_c \rightarrow \infty}, \quad (18)$$

so that  $\mu_B = M_B$  at large  $N_c$ . Accordingly the pressure is small,  $\mathcal{P} = \mu_B n_B - \varepsilon \sim n_B^{5/3} / M_B \sim 1/N_c$ , as expected from purely baryonic matter in an ideal gas regime. This trend changes when quark states at low momenta get saturated, as we will see in the next section.

#### IV. QUARK MATTER FORMATION

We have seen that the quark states at low momenta begin to be saturated at  $n_B^c \sim \Lambda^3$ . Beyond this critical density we can no longer use the ideal gas description of baryons, and in fact the EoS behaves very differently before and after the saturation; EoS are much stiffer after the saturation.

We are not accustomed to how baryon momentum distribution  $\mathcal{B}$  should behave after the saturation. In this situation, instead of starting with  $\mathcal{B}$ , it is more intuitive to postulate the form of quark occupation probability  $f_q$  for which we can implement the quark Pauli blocking easily. In Sec.V, we will come back to the question of how  $\mathcal{B}$  looks like for the postulated form of  $f_q$ .

#### A. A model of saturation

We assume that the occupation probability changes smoothly just after the saturation takes place. As a trial, we postulate the form

$$f_q^{\text{after}} = \theta(p_{\text{sat}} - p) + \theta(p - p_{\text{sat}}) f_q(p - p_{\text{sat}}; n_B^c), \quad (19)$$

where  $p_{\text{sat}}$  is a function of  $n_B$ . The first term is responsible for states occupied with the probability 1; the states to  $p = p_{\text{sat}}$  are saturated. Meanwhile the second term is for states with  $p > p_{\text{sat}}$  which are only partially occupied. Here we assume that the distribution  $f_q$  at  $n_B^c$  is shifted by the occupied level, so the states up to  $\sim p_{\text{sat}} + \Lambda$  can be occupied with substantial probability. For  $\Lambda \rightarrow 0$ , the postulated form of  $f_q$  is reduced to the form for the ideal quark gas. But we keep  $\Lambda$  finite, assuming that quarks just after the saturation are not fully delocalized. The behavior of  $f_q$  after the saturation is shown in Fig.1 for  $n_B/n_0 > 1.25$  with  $\Lambda = 0.25$  GeV.

While the postulated form of  $f_q$  seems a small departure from  $f_q$  in a baryonic matter, it has dramatic impacts on the EoS. First we note that the baryon density before and after the saturation are continuous, as we postulate the continuous changes in  $f_q$ . The relation between the Fermi momentum and  $p_{\text{sat}}$  is given by

$$\begin{aligned} \frac{P_F^3}{6\pi^2} &= \frac{p_{\text{sat}}^3}{6\pi^2} + \frac{1}{2\pi^2} \int_{p_{\text{sat}}}^{\infty} p^2 dp f_q(p - p_{\text{sat}}; n_B^c) \\ &= \frac{p_{\text{sat}}^3}{6\pi^2} + \frac{1}{2\pi^2} \int_0^{\infty} (p + p_{\text{sat}})^2 dp f_q(p; n_B^c). \end{aligned} \quad (20)$$

Near the saturation, we keep only terms to  $O(p_{\text{sat}})$ .

$$\frac{P_F^3}{6\pi^2} \simeq \frac{(P_F^c)^3}{6\pi^2} + \frac{p_{\text{sat}} \Lambda_c^2}{2\pi^2}, \quad (21)$$

or

$$p_{\text{sat}} \simeq \frac{\pi^2 (n_B - n_B^c)}{N_f \Lambda_c^2}, \quad (22)$$

where  $\Lambda_c \sim \Lambda$  characterizes the thickness of the distribution at  $n_B = n_B^c$ ,

$$\Lambda_c^2 = \int_0^{\infty} dp^2 f_q(p; n_B^c). \quad (23)$$

In the large  $N_c$ ,  $f_q(p; n_B^c) = e^{-\tilde{p}^2}$  so that  $\Lambda_c \rightarrow \Lambda$ . It is clear that  $p_{\text{sat}} \rightarrow 0$  as  $n_B \rightarrow n_B^c$  from above. Similarly  $\varepsilon$  is continuous before and after the saturation,

$$\varepsilon = \varepsilon_{\text{sat}} + \frac{N_c N_f}{\pi^2} \int_{p_{\text{sat}}}^{\infty} p^2 dp E_q(p) f_q(p - p_{\text{sat}}; n_B^c). \quad (24)$$

where  $\varepsilon_{\text{sat}}$  is the contribution from  $p = 0$  to  $p_{\text{sat}}$ . For a small  $p_{\text{sat}} \sim 0$ , we neglect  $\varepsilon_{\text{sat}}$  and expand the integrand in the second term,

$$\varepsilon \simeq \varepsilon_c + p_{\text{sat}} \frac{N_c N_f}{\pi^2} \int_0^{\infty} p^2 dp E_q(p) \left( - \frac{\partial f_q(p; n_B^c)}{\partial p} \right), \quad (25)$$

where  $\varepsilon_c$  is the energy density at  $n_B = n_B^c$ . The derivative  $\partial f_q / \partial p^2 \leq 0$ , so the  $\varepsilon$  approaches  $\varepsilon_c$  continuously from above for  $p_{\text{sat}} \rightarrow 0^+$ . Noting  $\partial p_{\text{sat}} / \partial n_B \simeq \pi^2 / N_f \Lambda_c^2$ , the chemical potential just after the saturation is

$$\mu_B \simeq \frac{N_c}{\Lambda_c^2} \int_0^\infty p^2 dp E_q(p) \left( - \frac{\partial f_q(p; n_B^c)}{\partial p} \right), \quad (26)$$

which will be compared to the  $\mu_B$  before the saturation.

A number of analytic insights are obtained in the large  $N_c$  limit, where  $f_q(p; n_B^c) \rightarrow e^{-\tilde{p}^2}$  and  $\Lambda_c \rightarrow \Lambda$ , so that

$$\frac{\mu_B^{\text{after}}}{N_c} \rightarrow 2\Lambda \int_0^\infty \tilde{p}^3 d\tilde{p} \tilde{E}_q(p) e^{-\tilde{p}^2}, \quad (27)$$

where we wrote  $\tilde{E} = E/\Lambda$ . The chemical potential before the saturation is given by the baryon mass at large  $N_c$ ,

$$\frac{\mu_B^{\text{before}}}{N_c} \rightarrow \frac{4\Lambda}{\sqrt{\pi}} \int_0^\infty \tilde{p}^2 d\tilde{p} \tilde{E}_q(p) e^{-\tilde{p}^2} = M_B. \quad (28)$$

If the saturation takes place in the relativistic regime of quarks, we may expand  $E_q \sim p + \dots$ , and find

$$\frac{\mu_B^{\text{after}}}{\mu_B^{\text{before}}} \rightarrow \frac{\sqrt{\pi}}{2} \left( \frac{3\sqrt{\pi}}{4} + \dots \right) \simeq 1.18 + \dots, \quad (29)$$

where the chemical potential jumps by  $\simeq 0.18M_B$ . Meanwhile, in the non-relativistic limit,

$$\left( \frac{\mu_B^{\text{after}}}{\mu_B^{\text{before}}} \right)_{\text{NR}} \rightarrow 1 + \frac{\Lambda^2}{4M_q^2} + \dots, \quad (30)$$

where the jump in  $\mu_B$  is the order of non-relativistic corrections.

We found that, while  $n_B$  and  $\varepsilon$  do not contain any jumps, the derivatives do. Of course, the thermodynamics does not allow jumps in  $\mu_B$  and the results being presented must contain something unphysical, in spite of the seemingly reasonable form of  $f_q$  in Eq.(19). But for the moment we proceed further to examine what would happen in this idealized description.

Fig.3 shows  $\mu_B$  as function of  $n_B/n_0$  where we chose  $N_c = 3$ ,  $M_q = 0.3$  GeV, and  $\Lambda = 0.25$  GeV, for which  $M_B \simeq 1.26$  GeV, and the jump in  $\mu_B$  associated with the saturation is  $\simeq 0.1$  GeV. It is clear that the  $\mu_B$  and  $\varepsilon/n_B$  after the saturation grow much faster than the behavior before the saturation. For comparisons, we also show the results for the QHC19-D EoS [38] as an example of EoS consistent with NS observations; for the QHC19-D,  $M_{\text{max}} \simeq 2.28M_\odot$ ,  $R_{1.4} \simeq 11.6$  km, and  $R_{2.08} \simeq 11.5$  km. (In Sec.VII we will make comparisons again after adjusting the baryon mass.)

These jumps in  $\mu_B$  result in the discontinuities in the corresponding pressure  $\mathcal{P}$  through the thermodynamic relation  $\mathcal{P} = \mu_B n_B - \varepsilon$ , where  $n_B$  and  $\varepsilon$  are continuous but  $\mu_B$  are not. Now the pressure just after the saturation is

$$\mathcal{P} \simeq \mu_B^{\text{after}} n_B - \varepsilon \simeq (\mu_B^{\text{after}} - \mu_B^{\text{before}}) n_B^c \sim N_c \Lambda^4, \quad (31)$$

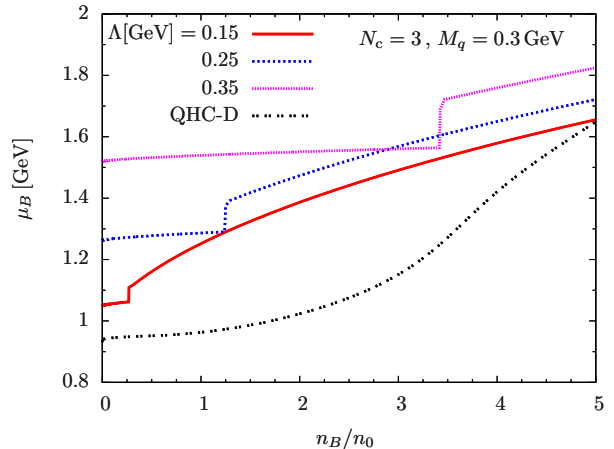


FIG. 3. The  $n_B$  dependence of the baryon chemical potential  $\mu_B$  for a model Eq.(19) without interactions. The results of  $N_c = 3$ ,  $M_q = 0.3$  GeV, and  $\Lambda = 0.15, 0.25, 0.35$  GeV are shown. QHC-D is also plotted as a reference.

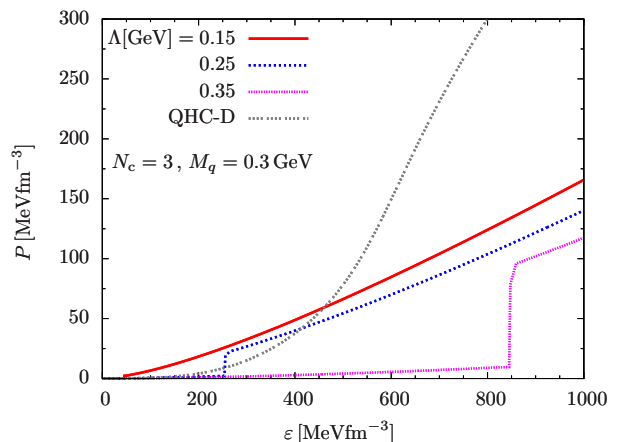


FIG. 4. The  $\mathcal{P}$  vs  $\varepsilon$  for the setup same as Fig.3.

which is much bigger than the pressure of an ideal baryon gas,  $\mathcal{P} \sim n_B^{5/3} / M_B \sim (P_F / \Lambda)^3 / N_c$ . Accordingly the squared speed of sound  $c_s^2 = \partial \mathcal{P} / \partial \varepsilon$  diverges to  $+\infty$  at the saturation. The  $\mathcal{P}$  vs  $\varepsilon$  for the setup same as Fig.3 is shown in Fig.4. The early onset of the saturation leads to low density EoS stiffer than nuclear matter (QHC19 at  $n_B \lesssim 2n_0$  is given by the Togashi nucleonic EoS). Meanwhile our non-interacting model for quarks is not as stiff as the QHC19 at high density, and in fact the model is too soft to lead to the  $2M_\odot$  NSs.

## B. Smoothing out the discontinuities

The discontinuities are the artifacts which are presumably associated with our use of the ideal baryon gas picture for baryons just before the saturation. In conventional baryonic matter, interactions of  $O(N_c)$  are important, and the pressure before the saturation to increase

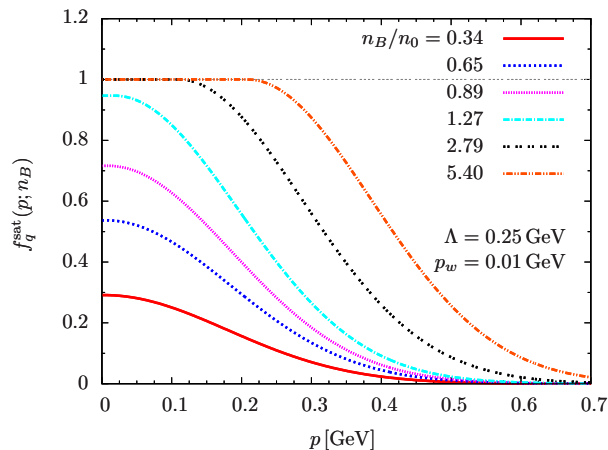


FIG. 5. The quark occupation probability for  $f_q^{\text{sat}}(p; n_B)$  in Eq.(32), for various  $n_B/n_0$ . We took  $\Lambda = 0.25$  GeV,  $p_w = 0.01$  GeV, and  $N_c = 3$ .

faster than in the ideal baryon gas. It should reduce the mismatch in  $\mu_B$  and  $\mathcal{P}$  before and after the saturation.

Technically, there is a simple way to smooth out the discontinuities. We consider a model

$$f_q^{\text{sat}}(p; p_{\text{sat}}) = \tanh(p_{\text{sat}}/p_w) \times [\theta(p_{\text{sat}} - p) + \theta(p - p_{\text{sat}}) e^{-(\tilde{p} - \tilde{p}_{\text{sat}})^2}], \quad (32)$$

where  $p_w$  is a regulator which should be taken to be very small,  $p_w \ll \Lambda$ . For  $p_{\text{sat}} \ll p_w$ ,  $p_{\text{sat}}$  in the step function and the Gaussian factor is negligible, so we can regard

$$f_q^{\text{sat}} \simeq \frac{p_{\text{sat}}}{p_w} e^{-\tilde{p}^2} \sim \frac{p_{\text{sat}}}{p_w} f_q(p; n_B = 0), \quad (33)$$

in computations of thermodynamic quantities. Technically, the factor  $p_{\text{sat}}/p_w \ll 1$  plays the role similar to the factor  $\sim \mathcal{N}P_F^3 \sim n_B/n_B^c$  in Eq.(12); there the shape of  $f_q$  was fixed but its magnitude increases until the saturation takes place. When  $p_{\text{sat}} \sim p_w$ , the model goes back to the model in Eq.(19) modulo  $\tilde{P}_F \sim 1/N_c$  corrections. The  $n_B$ -dependence of  $f_q^{\text{sat}}$  for  $p_w = 0.01$  GeV is shown in Fig.7. The qualitative behaviors are very similar to Fig.1 (the major difference comes from our neglect of  $\tilde{P}_F$  corrections in Eq.(32) compared to Eq.(19)).

Now we use  $f_q^{\text{sat}}$  to examine several thermodynamic quantities. Shown in Fig.6 is  $\mu_B$  as a function of  $n_B$ . Working with a model with the same form from low to high density, the artificial discontinuities found in the previous treatment are smoothed out, and  $\mu_B$  is now continuous, as it should. Accordingly, the (squared) speed of sound  $c_s^2$  is now regulated and well-defined, as shown in Fig.7. The  $c_s^2$  has a peak around the density where the saturation effects become important, and it exceeds the conformal value  $1/3$  for a sufficiently small  $p_w$ . The degree of the smearing is rather sensitive to the value of  $p_w$ , and too small  $p_w$  tends to violate the causality constraint  $c_s^2 \leq 1$ . The sharpness of the peak should be dynamically determined by the interplay of baryon and

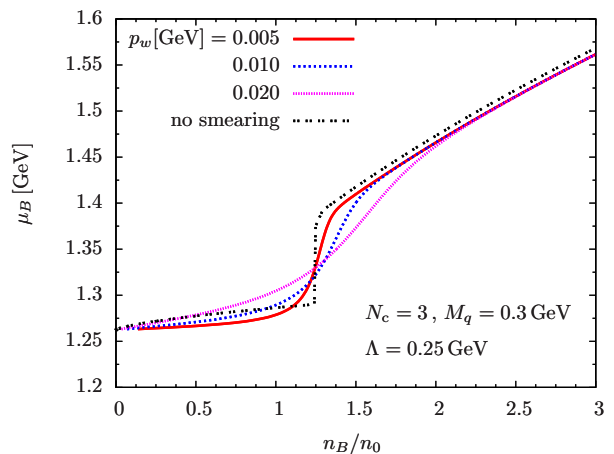


FIG. 6. The  $\mu_B$  vs  $n_B/n_0$  for the  $p_w = 0.005, 0.010, 0.020$  GeV. We took  $\Lambda = 0.25$  GeV,  $M_q = 0.3$  GeV, and  $N_c = 3$ .

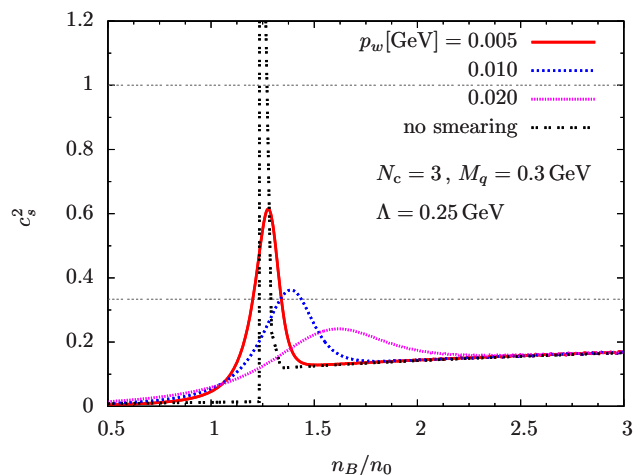


FIG. 7. The squared speed of sound  $c_s^2$  vs  $n_B/n_0$  for the parameter set same as Fig.6.

quark dynamics. We will choose  $p_w = 0.01 - 0.02$  GeV unless otherwise stated.

Finally we note the conceptual aspect of the saturation model  $f_q^{\text{sat}}$  in the form of Eq.(32). While we introduced the model with  $p_w$  just as a technical device to handle the artificial discontinuities in  $\mu_B$ , it is interesting to see that introduction of small probability of the saturated state led to reasonable smooth behaviors in thermodynamic quantities. The saturation at very low momentum in dilute regime  $n_B \ll \Lambda^3$  may not be entirely unrealistic for interacting baryons, as their long range interactions (meson exchanges) are mediated by quark exchanges in the color-singlet channel. Such scenario was discussed in the context of mode-by-mode percolation or soft deconfinement [77].

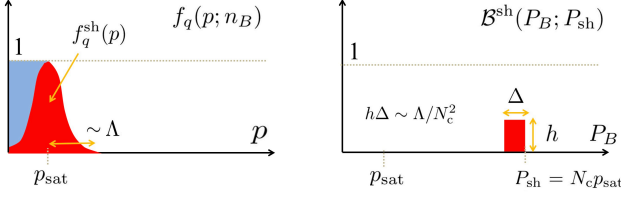


FIG. 8. A model  $\mathcal{B}^{\text{sh}}$  for a baryon momentum distribution after the saturation takes place. The  $\mathcal{B}^{\text{sh}}$  convoluted with  $Q_{\text{in}}$  leads to the quark momentum distribution  $f_q^{\text{sh}}$  around  $p_{\text{sat}}$ . For the “baryon shell” of  $\mathcal{B}^{\text{sh}}$ , we found  $h\Delta \sim \Lambda/N_c^2$  for  $P_{\text{sh}} \sim N_c\Lambda$ . If we fix  $h = 1$ , the thickness  $\Delta$  gets narrower as in the MR model.

## V. BARYONS AFTER SATURATION

As we have seen, the saturation of low momentum quark states induces a rapid increase in the pressure. Such changes are difficult to imagine from purely baryonic descriptions, and we are interested in how the corresponding occupation probability of baryon states ( $\mathcal{B}$ ) looks like. Through attempts to understand  $\mathcal{B}$ , we also discuss how to obtain expressions similar to the MR model for quarkyonic matter equations of state [47].

Regarding  $f_q$  and  $\mathcal{B}$  as vectors for a given  $n_B$ , they are related through a matrix  $Q_{\text{in}}$  as

$$\vec{f}_q = Q_{\text{in}} \vec{\mathcal{B}}, \quad (34)$$

where  $0 \leq \mathcal{B}(P_B; n_B) \leq 1$  for any  $P_B$  and  $n_B$ . The equation is linear and in principle one can take inversion to determine  $\mathcal{B}$  for a given  $f_q$ . But in practice this method does not work well. Another strategy is to prepare some model  $\mathcal{B}_\alpha$  for  $\mathcal{B}$  with parameters  $\vec{\alpha} = (\alpha_1, \alpha_2, \dots)$ , and minimize a function “energy” functional

$$\mathcal{H}(\vec{\alpha}) = (\vec{f}_q - Q_{\text{in}} \vec{\mathcal{B}}_\alpha)^T (\vec{f}_q - Q_{\text{in}} \vec{\mathcal{B}}_\alpha) + \mathcal{I}_{\text{cost}}(\mathcal{B}_\alpha), \quad (35)$$

where  $\mathcal{I}_{\text{cost}}$  is some functional which gives the energetic penalty if, for instance,  $\mathcal{B}_\alpha$  violates the condition  $0 \leq \mathcal{B}(P_B; n_B) \leq 1$ . For this strategy to work, we need a good guess for the form of  $\mathcal{B}$ .

For this purpose, we first assume baryons with momenta  $P_B \gtrsim \Lambda$  and which form of  $f_q$  resulted in. We consider the form

$$\mathcal{B}^{\text{sh}}(P_B; P_{\text{sh}}) = h\theta(P_{\text{sh}} - P_B)\theta(P_B - P_{\text{sh}} - \Delta), \quad (36)$$

where “sh” is the abbreviation of “shell”, and  $h$  is the overall size in the occupation probability for states with momenta  $P_{\text{sh}} - \Delta (\geq 0)$  to  $P_{\text{sh}}$  and must satisfy  $0 \leq h \leq 1$ . Integrating the baryon momentum distribution, we get the contribution to  $f_q$  as

$$f_q^{\text{sh}}(p) \simeq h\Delta \frac{N_c^3}{\sqrt{\pi}} \frac{\tilde{P}_{\text{sh}}}{\tilde{p}} e^{-\tilde{p}^2 - \tilde{P}_{\text{sh}}^2} (e^{2\tilde{p}\tilde{P}_{\text{sh}}} - e^{-2\tilde{p}\tilde{P}_{\text{sh}}}) \quad (37)$$

where we set  $\tilde{P}_{\text{sh}} = P_{\text{sh}}/N_c\Lambda$ . For small  $\tilde{p}\tilde{P}_{\text{sh}}$ ,

$$f_q^{\text{sh}}(p) \sim 4h\Delta \frac{N_c^2}{\sqrt{\pi}} e^{-\tilde{p}^2 - \tilde{P}_{\text{sh}}^2} \tilde{P}_{\text{sh}}^2 (1 + O(\tilde{p}^2 \tilde{P}_{\text{sh}}^2)), \quad (38)$$

and for large  $\tilde{p}\tilde{P}_{\text{sh}}$ ,

$$f_q^{\text{sh}}(p) \simeq h\Delta \frac{N_c^2}{\sqrt{\pi}} \frac{\tilde{P}_{\text{sh}}}{\tilde{p}} e^{-(\tilde{p} - \tilde{P}_{\text{sh}})^2}, \quad (39)$$

where the maximum of  $f_q$  appears at  $\tilde{p} \sim \tilde{P}_{\text{sh}}$ .

Below we examine these asymptotic behaviors in some details. We can see a number of the remarkable features in the large  $N_c$  limit. For  $P_{\text{sh}} \sim \Lambda$  or  $\tilde{P}_{\text{sh}} \sim 1/N_c$ , we use Eq.(38) to obtain

$$f_q^{\text{sh}}(p) \sim h\Delta e^{-\tilde{p}^2}, \quad (40)$$

where the condition  $f_q \leq 1$  demands  $h\Delta \sim 1$ .

For  $P_{\text{sh}} \sim N_c\Lambda$  or  $\tilde{P}_{\text{sh}} \sim 1$ , we use Eq.(39) to obtain

$$f_q^{\text{sh}}(p) \sim h\Delta N_c^2 e^{-(\tilde{p} - \tilde{P}_{\text{sh}})^2}, \quad (41)$$

where we set  $\tilde{P}_{\text{sat}}/\tilde{p} \sim 1$  as the Gaussian part has a peak at  $\tilde{p} = \tilde{P}_{\text{sh}}$ . In this regime the condition  $f_q \leq 1$  demands  $h\Delta \sim \Lambda/N_c^2$ .

Now we consider the forms of  $h$  that are compatible with the scaling behaviors in Eqs.(40) and (41). For example, one can take

$$[h\Delta](P_{\text{sh}}) \sim c_0\Lambda \left( \frac{\Lambda^2}{P_{\text{sh}}^2} + \frac{c_1}{N_c} \frac{\Lambda}{P_{\text{sh}}} + \frac{c_2}{N_c^2} \right), \quad (42)$$

where  $c_0, c_1$ , and  $c_2$  are constants of  $O(1)$ . For  $P_{\text{sh}} \sim \Lambda$ , the first term dominates. For  $P_{\text{sh}} \sim N_c\Lambda$ , all these three terms can be comparable. In what follows, baryon states with large momenta  $P_{\text{sh}}$  are compatible with the condition  $f_q \leq 1$  only if those states are occupied with the small probability density, i.e., either  $h$  or  $\Delta$  becomes small for large  $P_{\text{sh}}$ . In particular baryon states with momenta  $\sim N_c\Lambda$  are occupied with a small but nonzero probability  $h\Delta \sim 1/N_c^2$ .

Now we notice that the scaling  $f_q^{\text{sh}} \sim e^{-(\tilde{p} - \tilde{P}_{\text{sh}})^2}$  is similar to the behavior of  $f_q(p - p_{\text{sat}}; n_B^c) \sim e^{-(\tilde{p} - \tilde{p}_{\text{sat}})^2}$  in Eq.(19) for the partially occupied quark states beyond the saturated states. This suggests that  $\tilde{P}_{\text{sh}} \simeq \tilde{p}_{\text{sat}}$  or  $P_{\text{sh}} \simeq N_c p_{\text{sat}}$ , and the approximate relation

$$f_q(p - p_{\text{sat}}; n_B^c) \sim \int_{P_B} Q_{\text{in}} \mathcal{B}^{\text{sh}}(P_B; P_{\text{sh}} \simeq N_c p_{\text{sat}}). \quad (43)$$

Thus the shell form Eq.(36) turns out to be a good candidate for the  $p > p_{\text{sat}}$  part of the quark distribution  $f_q$  postulated in Eq.(19). The schematic picture is given in Fig.8.

Substituting this form into Eq.(19), and then integrating quark momenta  $p$ , we reach a model similar to the model of McLerran-Reddy [47]<sup>2</sup>. With  $P_{\text{sh}} = N_c p_{\text{sat}}$ , the

<sup>2</sup> Our presentation here is slightly different from the paper of McLerran and Reddy [47] where the concept of the occupation probability for baryons is not used, so  $h = 1$  from the very be-

baryon density and energy density per flavor are

$$\begin{aligned} \frac{n_B}{N_f} &\simeq \frac{h}{\pi^2} \int_{P_{\text{sh}}-\Delta}^{P_{\text{sh}}} dP_B P_B^2 + \frac{P_{\text{sat}}^3}{3\pi^2} \\ \frac{\varepsilon}{N_f} &\simeq \frac{h}{\pi^2} \int_{P_{\text{sh}}-\Delta}^{P_{\text{sh}}} dP_B P_B^2 E_B + N_c \int_0^{P_{\text{sat}}} \frac{dp p^2}{\pi^2} E_q(p), \end{aligned} \quad (45)$$

where we have used the relations  $\int_{\mathbf{p}} Q_{\text{in}} = 1$  and  $E_B(P_B) = N_c \int_{\mathbf{p}} Q_{\text{in}}(\mathbf{p}, \mathbf{P}_B) E_q(p)$ , and neglected possible double counting in  $f_q$  at  $p \lesssim p_{\text{sat}}$  which should be minor effects unless  $p_{\text{sat}}$  is very large. We also note that

$$\begin{aligned} \mu_B &= \frac{\partial P_{\text{sh}}}{\partial n_B} \frac{\partial \varepsilon}{\partial P_{\text{sh}}}, \\ &\simeq \frac{P_{\text{sh}}^2 E_B(P_{\text{sh}}) - (P_{\text{sh}} - \Delta)^2 E_B(P_{\text{sh}} - \Delta)}{P_{\text{sh}}^2 - (P_{\text{sh}} - \Delta)^2} \end{aligned} \quad (46)$$

where the contributions from the saturated quark states are suppressed by an extra factor of  $1/N_c$ . When  $P_{\text{sh}} \sim \Lambda$ , baryons are non-relativistic,  $E_B(P_{\text{sh}} - \Delta) \simeq E_B(P_{\text{sh}})$  and  $\mu_B - M_B \simeq E_B(P_{\text{sh}}) - M_B \sim 1/N_c$ . As  $P_{\text{sh}}$  approaches  $N_c \Lambda (\gg \Delta)$ , we find  $\mu_B - M_B \simeq E_B(P_{\text{sh}}) - M_B + (P_{\text{sh}}/2) \partial E_B / \partial P_{\text{sh}} \sim P_{\text{sh}}^2 / E(P_{\text{sh}}) \sim N_c \Lambda$ , as in usual relativistic expressions.

What is remarkable is that the relativistic regime is reached for  $n_B \sim \Lambda^3$ . For  $P_{\text{sh}} \sim N_c \Lambda$ , we obtain

$$\begin{aligned} n_B &\simeq \frac{h}{\pi^2} (P_{\text{sh}}^3 - (P_{\text{sh}} - \Delta)^3) \sim h \Delta P_{\text{sh}}^2 \\ &\simeq c_0 \Lambda^3 + c_1 \Lambda^2 \frac{P_{\text{sh}}}{N_c} + c_2 \Lambda \left( \frac{P_{\text{sh}}}{N_c} \right)^2, \end{aligned} \quad (47)$$

which is  $\sim \Lambda^3$ . For small  $P_{\text{sh}}$ , the first term dominates, while the second and third terms slowly grow as  $P_{\text{sh}}$  becomes  $\sim N_c \Lambda$ . This result drastically differs from naive expectation  $n_B \sim (N_c \Lambda)^3$ . In ordinary baryonic descriptions at  $n_B \sim \Lambda^3$ , baryons approach the relativistic regime by interactions of  $O(N_c)$ , but here we found that relativistic baryons can also emerge just due to the constraints on baryons as composite particles. This reproduces the remarkable findings by McLerran and Reddy [47].

## VI. QUANTUM NUMBERS

We discuss the quantum numbers of baryons such as colors, flavors, and spins. The question is how baryons

---

ginning, while they assumed the form of  $\Delta$  to be

$$\Delta = \frac{\Lambda^3}{P_{\text{sh}}^2} + \frac{\kappa \Lambda}{N_c}. \quad (44)$$

The second term plays important roles to regulate  $\mu_B$  and the speed of sound.

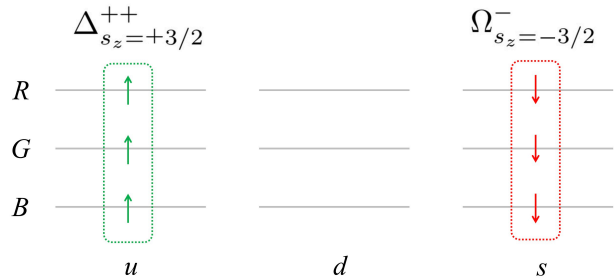


FIG. 9. Examples of quantum numbers for baryons where  $\Delta_{s_z=+3/2}^{++}$  and  $\Omega_{s_z=-3/2}^-$  are shown. The former (latter) fills the  $u \uparrow$  ( $d \downarrow$ ) states for all colors  $RGB$ , while leave the other color-flavor-spin states empty. For a given space wavefunction for quarks, six baryon states completely fill color-flavor-spin states.

saturate these quantum numbers for quark states. In previous sections we implicitly assumed that the quark states for  $N_c$  colors,  $N_f$  flavors, and two spins, are saturated by putting  $N_f$  species of baryons with two spins. In this section we explain why this description should be valid. Specifically we consider the  $N_c = N_f = 3$  cases to utilize the terminology common in hadron spectroscopy. We also ignore the mass difference among up-, down- and strange-quarks.

The argument is simplified by assuming  $SU(2N_f)$  symmetry in which there are no energy difference associated with spins and flavors. In particular nucleons,  $\Delta$ ,  $\Omega$ , so on, are all energetically degenerate. It is useful to focus on the following states,

$$\begin{aligned} \Delta_{s_z=\pm 3/2}^{++} &= [u_R \uparrow u_G \uparrow u_B \uparrow], [u_R \downarrow u_G \downarrow u_B \downarrow], \\ \Delta_{s_z=\pm 3/2}^- &= [d_R \uparrow d_G \uparrow d_B \uparrow], [d_R \downarrow d_G \downarrow d_B \downarrow], \\ \Omega_{s_z=\pm 3/2}^- &= [s_R \uparrow s_G \uparrow s_B \uparrow], [s_R \downarrow s_G \downarrow s_B \downarrow], \end{aligned} \quad (48)$$

where quark states are totally anti-symmetrized.

While there are much more S-wave baryons with spin or flavor excitations (such as baryon octet or decuplet), for given spatial wavefunctions we can saturate quark states using only the  $2N_f (= 6)$  states listed in Eq.(48). For example, by putting  $\Delta_{s_z=3/2}^{++}$ , colors  $RGB$  for up-quarks with spins aligned in  $\uparrow$ -directions are filled at once. Therefore the number of baryon species we need is the same as the number of quark species, as we have assumed in the previous sections. The arguments are applicable to any  $N_c$ .

This discussion also suggests that, once baryons with a specific spin-flavor quanta forms its Fermi sea, the other baryons cannot freely enter the system due to the Pauli blocking at quark level. For instance when  $\Delta_{s_z=3/2}^{++}$  and  $\Delta_{s_z=-3/2}^{++}$  form the large Fermi sea of up-quarks, one cannot put nucleons ( $uud$  or  $ddu$ ) at low energy, but must place them on top of the saturated Fermi sea. This viewpoint should be important when we discuss how hyperons enter dense nuclear matter. Also, this consideration should affect the treatment in the self-energy processes



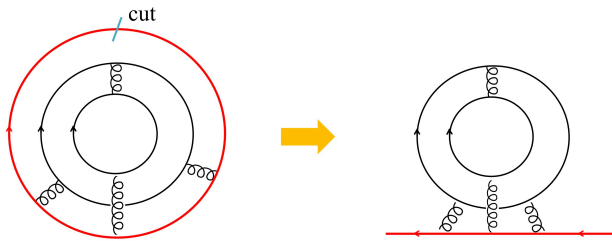


FIG. 10. A self-energy graph for a quark in a baryon. The gluon exchanges happen in the color anti-symmetric channels.

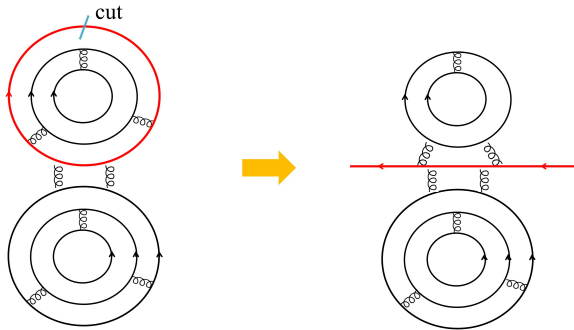


FIG. 11. A self-energy graph for a quark participating in baryon-baryon interactions. The gluon exchanges can happen in both the color anti-symmetric and symmetric channels.

for protons and neutrons, as virtual states are blocked by pre-occupied states.

More realistically we need to discuss the cases where protons and neutrons appear as the lowest energy states. Treatments of quantum numbers are more involved than the idealized ( $\Delta^{++}$ ,  $\Delta^-$ ,  $\Omega^-$ ) baryon bases used here. We leave such realistic cases for our future work.

## VII. INTERACTIONS

So far our discussions on EoS are entirely based on quasiparticle pictures, based on either quarks or baryons; the interactions for quarks have been taken into account only indirectly, by demanding that quark momentum are distributed to some range as they should localize by confining effects. Now we perturb the calculations presented in the previous sections. We discuss interactions in quark descriptions.

In principle, one can construct EoS from the information of single particle propagators. The pressure at given  $\mu_B$  is given by

$$\mathcal{P}(\mu_B) = \int_0^{\mu_B} d\mu'_B n_B(\mu'_B), \quad (49)$$

where  $n_B$  can be expressed as

$$n_B(\mu_B) = \frac{1}{N_c} \text{Tr}[S_q], \quad (50)$$

where  $S_q$  is the quark propagator and the trace runs over all quantum numbers. This relation is exact for whatever interactions; for example, in functional frameworks such as the 2PI action [78–80], Eq.(50) always follows from self-consistent treatments of the quark self-energy and interactions. As a result, the effects of interactions can be included into the self-energy of the propagator. If we need to include the baryon-baryon interactions, one should write the corresponding 2PI graphs and consider all possible cuts of quark propagators to generate the self-energy graph, see Fig.10 for a quark in a baryon and Fig.11 for a quark participating in baryon-baryon interactions.

In this paper we simply assume a phenomenological parameterization for a single quark energy. We consider the form for a single particle energy,

$$E_q(p; f_q) = \sqrt{p^2 + M_q^2} + \mathcal{V}[f_q], \quad (51)$$

where  $\mathcal{V}$  is the contribution from interactions that may depend on  $f_q$ .

Our first task is to adjust the baryon mass. As in a quark model with a phenomenological confining potential [70, 71], our baryon mass is too massive due to the kinetic energies of localized quarks. To reproduce the observed baryon spectra, we need color-electric interactions for the overall reduction in the masses for baryons, and color-magnetic interactions to get the correct mass splitting, e.g., the  $N$ - $\Delta$  and  $\pi$ - $\rho$  splittings. In this work we focus on the electric interaction but neglecting the details of mass splittings. In vacuum, we consider

$$\mathcal{V}_{\text{CE}}^{\text{vac}}[f_q] = -C_E^{\mathcal{A}} (\leq 0), \quad (52)$$

where  $\mathcal{A}$  indicates an anti-symmetric representation in colors. We will adjust  $\mathcal{V}_{\text{CE}}^{\text{vac}}$  to set the baryon mass to the nucleon mass,  $M_N \simeq 939$  MeV.

In a baryon, the color-electric forces always reduce the average quark energy, as the color-wavefunction is always anti-symmetric for any combinations of quarks (e.g., Fig.10). For symmetric wavefunctions, the color-electric forces yield repulsive forces, and such channels are inevitable when several baryons come close together (e.g., Fig.11).

To take into account these attractive forces in the dilute regime and the repulsive forces in denser regime, we consider the parameterization ( $C_E^{\mathcal{S}} \geq 0$ )

$$\mathcal{V}_{\text{CE}}[f_q] = -C_E^{\mathcal{A}} \times (1 - \gamma f_q^\beta) + C_E^{\mathcal{S}} f_q^\beta, \quad (53)$$

where  $\mathcal{S}$  indicates symmetric channels in colors. The power  $\beta$  controls the impacts of partially occupied levels, and the parameter  $\gamma$  will be chosen to either 0 or 1 to examine the effects of partially filled states.

In this model quarks with  $p \gg p_{\text{sat}}$  are free from the saturated levels, and have the energy reduction,

$$\mathcal{V}_{\text{CE}}[f_q] \simeq -C_E^{\mathcal{A}}, \quad (54)$$

as quarks in a baryon. This feature may be interpreted as the attractive correlations near the Fermi surface;

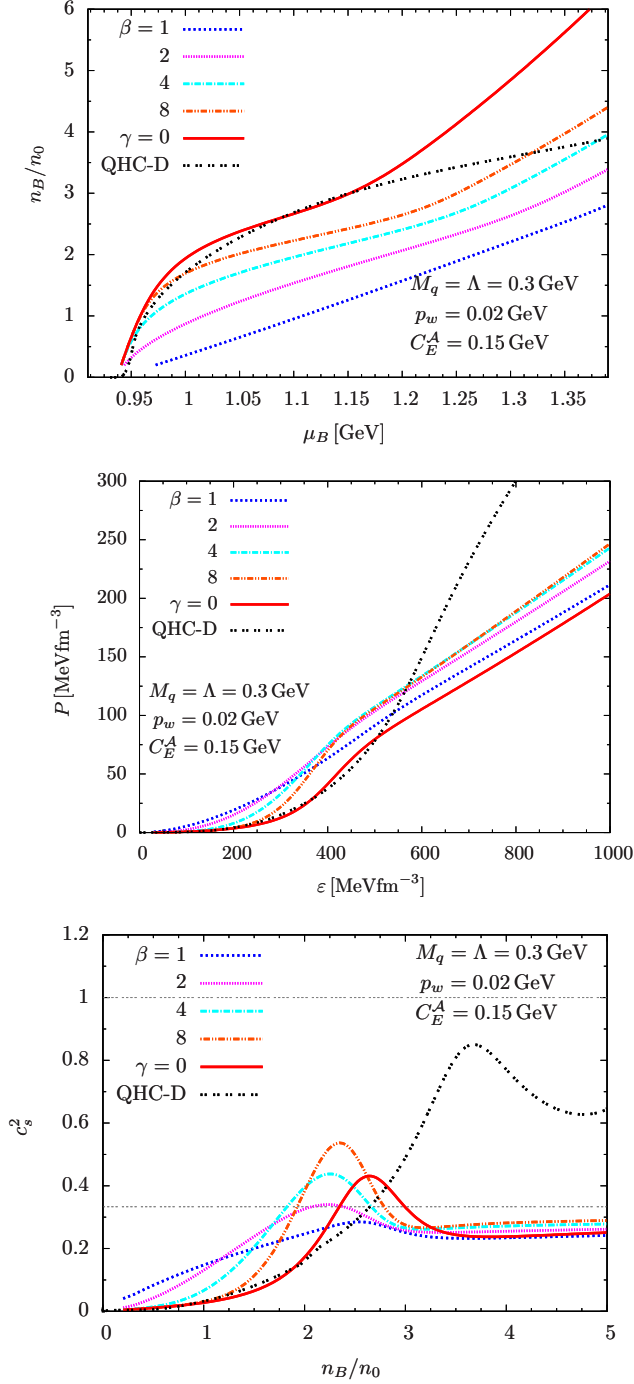


FIG. 12. Equations of state,  $n_B$  vs  $\mu_B$ ,  $\mathcal{P}$  vs  $\varepsilon$ , and  $c_s^2$  vs  $n_B$ , with  $C_E^A = 0.15$  GeV and  $C_E^S = 0$ . The impacts of partially filled states are examined for the power  $\beta = 1, 2, 4, 8$  with  $\gamma = 1$  or  $\gamma = 0$ . (Reminder: for the QHC19-D,  $M_{\max} \simeq 2.28M_\odot$ ,  $R_{1.4} \simeq 11.6$  km, and  $R_{2.08} \simeq 11.5$  km.)

since the quark states are not fully occupied, quarks can arrange themselves to enhance the portion of color-antisymmetric channels as in an isolated baryon. Meanwhile, quarks with  $p \ll p_{\text{sat}}$  have less freedom to arrange their wavefunctions, and feel the overall repulsion,

$$\mathcal{V}_{\text{CE}}[f_q] = -C_E^A \times (1 - \gamma) + C_E^S, \quad (55)$$

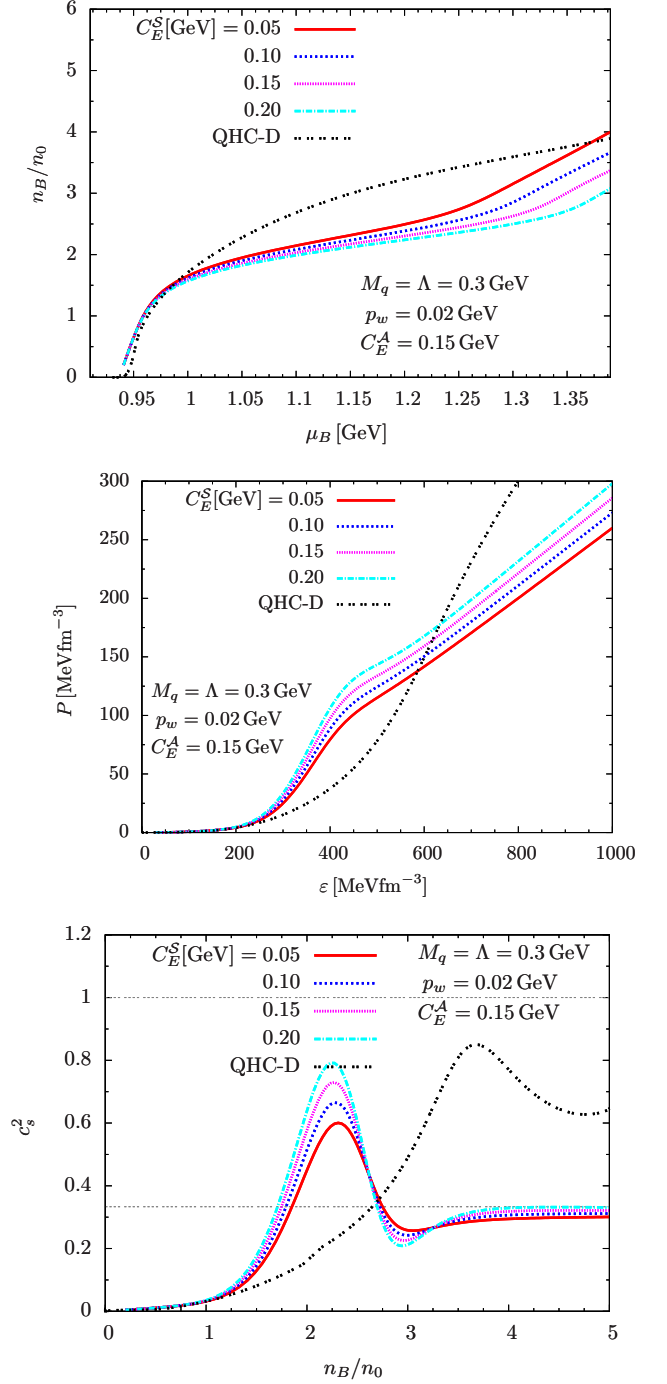


FIG. 13. The plots same as Fig.12 except  $\beta = 8$  is fixed and  $C_E^S$  is varied from 0.05 to 0.20 GeV.

due to the appearance of the repulsive channels. The repulsive energy is activated only when  $p_{\text{sat}}$  becomes substantial. The power  $\beta$  determines how sharply one can distinguish the filled ( $f_q \simeq 1$ ) and partially filled ( $f_q < 1$ ) states.

Now we put these ingredients into our numerical analyses. First we set  $C_E^S = \gamma = 0$ . Shown in Fig.12 are various EoS,  $n_B$  vs  $\mu_B$ ,  $\mathcal{P}$  vs  $\varepsilon$ , and  $c_s^2$  vs  $n_B$ , together with the results of QHC-D as a guideline for EoS con-

tent with the NS observations [38]. We set  $C_E^A = 0.15$  GeV to get  $M_B \simeq 0.94$  GeV at  $n_B = 0$ . The EoS at low density behaves as those in QHC19-D, but starts to deviate from QHC19 around  $n_B \sim 3n_0$  due to softening of our model at high density. The speed of sound has the maximum at  $\sim 2.6n_0$ , mainly determined by our model parameter  $\Lambda$  (or baryon size). We emphasize that stiffening takes place in our model solely by the saturation effects.

To get stiffer EoS at high density, we set  $\gamma = 1$  to activate the effects of partially filled states. With  $\beta = 1$ , the low density part is much stiffer than the baryonic part in the QHC19 (which is the Togashi EoS [15]), contradicting with nuclear EoS at  $n_B \lesssim n_0$ . Here quarks lost the attractive energy too rapidly, leading to rapid growth in  $\mu_B$  as  $n_B$  increases. One can delay the loss of attractive energies by increasing  $\beta$  and suppressing  $f_q^\beta$  terms for  $f_q < 1$ . We found that, for  $\beta \gtrsim 8$ , our EoS gets along with the nuclear EoS for  $n_B \lesssim 1.5n_0$ . Meanwhile, the high density part is considerably softer than QHC19-D.

In order to make the high density part stiffer, the simple way is to turn on  $C_E^S$ . We increase from  $C_E^S = 0.05$  GeV to 0.20 GeV, and the corresponding results are shown in Fig.13. The repulsive forces are activated only when  $f_q \simeq 1$ , or  $p_{\text{sat}}$  is large, so leaving the low density part as before, but stiffening the high density part where  $p_{\text{sat}}$  is substantial. The location of the maximum in the speed of sound is not very sensitive to the choice of  $C_E^S$ , but the height becomes larger for a greater  $C_E^S$ . We also note that the width of the peak is sensitive to our choice of  $p_w$ , as in Fig.7.

## VIII. SUMMARY

In this paper we discussed how quark degrees of freedom stiffen EoS. For the purpose to relate the quark dynamics for a single baryon to baryonic matter and quark matter formation, we have introduced a model that relates (squared) quark wavefunctions  $Q_{\text{in}}$  in a baryon and the occupation probability of states for baryons  $\mathcal{B}$  and quarks  $f_q$ . We also consider the effects of interactions at quark level.

Below we summarize our findings:

(i) In dilute regime, the confined quarks contribute to the energy density through the mass of baryons, but do not directly contribute to the pressure, hence the EoS are very soft (Fig.14 left). This dilute regime continues until the low momentum states for quarks are saturated (Fig.14 middle). The saturation can take place considerably before the baryons fully overlap, possibly at density close to the nuclear saturation density,  $n_B \sim 1 - 3n_0$ . This picture is in line with the recent proposal of Soft Deconfinement as the onset of the mode-by-mode percolation [77].

(ii) After the saturation, the energy per particle,  $\varepsilon/n_B$ , begins to change as in quark matter (Fig.14 right), and the pressure,  $\mathcal{P} = n_B^2 \partial(\varepsilon/n_B)/\partial n_B$ , grows rapidly, al-

though changes in  $n_B$  and  $\varepsilon$  are modest. This leads to a peak in speed of sound,  $c_s^2 = \partial\mathcal{P}/\partial\varepsilon$ . In our model such a peak follows by just assuming the continuity of  $f_q$  before and after the saturation, while no detailed descriptions of interactions were necessary.

(iii) To take into account the constraint  $f_q \leq 1$  after the saturation, it is the easiest to directly work with the quark description. But we can also infer the baryon momentum distribution  $\mathcal{B}$  consistent with the desired form of  $f_q$ . Through such attempts we reached a model similar to the MR model for quarkyonic matter. The resulting  $\mathcal{B}$  differs from the pure baryonic descriptions in which baryons are treated as if elementary particles; baryons after the saturation are highly relativistic.

(iv) We do not need many baryon species to fill the quark levels. For three-flavors, we need  $2N_f$  baryon states to fill the quark color-flavor-spin states for a given spatial wavefunction. In this respect, nucleons and hyperons should not be treated as independent when they share the same quark states [61, 81].

(v) While the stiffening of matter near the saturation seems a generic trend in our modeling, a model without interactions does not lead to sufficient stiffness at high density,  $n_B \gtrsim 4 - 5n_0$ , that is required by the existence of  $2M_\odot$  NSs. This observation is consistent with viewpoints in our previous works [38, 75, 82] where various short-range interactions of  $p = 0.2 - 1$  GeV were discussed. One way to stiffen the high density part is to use a model in which quarks in saturated states feel repulsions but those near the Fermi surface enjoy the attractive correlations.

Unfortunately, our discussions remain largely qualitative and the treatments of dynamics are in many senses ad hoc. There remain many things to be done, as listed below:

Firstly, it is better to directly use a quark wavefunction in a constituent quark model. The complication compared to the present work is that the correlations among quarks in a baryon are determined by the relative momenta, e.g.,  $\mathbf{p}_1 - \mathbf{p}_2$ , between a quark 1 and 2, rather than the difference from the average momentum  $\mathbf{P}_B/N_c$ .

Secondly, to use the framework for predict the NS properties, we need to include the flavor asymmetry, and in particular have to discuss how nucleons fill the quark states at low energy. The latter is rather involved as nucleon spin-flavor wavefunctions are in mixed representations, but should be doable.

Thirdly, as we use a quark model, it is desired to directly use interactions in a quark model for baryons. There have been many works to reproduce baryon properties, and the lattice QCD studies of baryon-baryon interactions support the idea that the short range part (such as the hard core repulsion among nucleons) is overall consistent with the descriptions based on quark dynamics with one-gluon exchanges.

Fourthly, pairing effects leading to the chiral condensates or diquark condensates should be discussed to determine the phase structures as well as EoS. In this work we fixed the constituent quark mass as in vacuum, but it

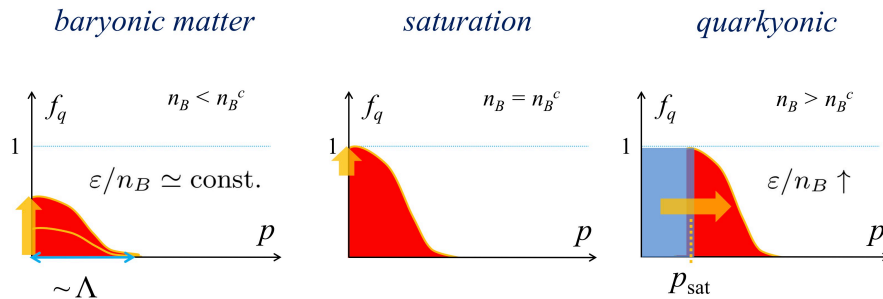


FIG. 14. A schematic picture for the evolution of matter from the baryonic to quark matter regime. In baryonic matter, the energy per particle is  $\epsilon/n_B \simeq \text{const.}$ , and after the saturation,  $\epsilon/n_B$  starts to grow as in quark matter. As the pressure is given by  $\mathcal{P} = n_B^2 \partial(\epsilon/n_B)/\partial n_B$ , matter after the saturation has much larger pressure than baryonic matter. The speed of sound makes a peak around the density where the saturation happens.

is very likely the effective mass changes with density.

Finally, the model should be extended to finite temperatures. When we come to thermal excitations, we will need to address whether thermal excitations are hadrons or quarks. In fact, this is a crucial step to establish the quark-hadron continuity or the quarkyonic matter scenario, because the response in EoS as well as in the transports to changes in temperature is entirely different for hadronic and quark excitations [83]. In two-color QCD there is a hint from the lattice QCD for hadronic excitations at high density [84, 85], although more data is needed to establish this idea.

In forthcoming papers we plan to give more quantitative estimates on EoS, arranging the setup for the baryon spectra and NS phenomenology.

## ACKNOWLEDGMENTS

I thank Larry D. McLerran and Robert D. Pisarski for having introduced me to the topic of quarkyonic matter; Dyana C. Duarte, Saul Hernandez-Ortiz, Kie Sang Jeong for instructions about quarkyonic matter equations of state; Kenji Fukushima and Wolfram Weise for discussions on Soft Deconfinement; Gordon Baym and Tetsuo Hatsuda for general discussions on neutron star equations of state; Daiki Suenaga for discussions on thermal excitations in quark matter. This work is supported by NSFC grant No. 11875144.

- 
- [1] N. Itoh, *Prog. Theor. Phys.* **44**, 291 (1970).
  - [2] J. C. Collins and M. J. Perry, *Phys. Rev. Lett.* **34**, 1353 (1975).
  - [3] K. Fukushima and T. Hatsuda, *Rept. Prog. Phys.* **74**, 014001 (2011), [arXiv:1005.4814 \[hep-ph\]](#).
  - [4] M. Buballa and S. Carignano, *Prog. Part. Nucl. Phys.* **81**, 39 (2015), [arXiv:1406.1367 \[hep-ph\]](#).
  - [5] M. G. Alford, A. Schmitt, K. Rajagopal, and T. Schäfer, *Rev. Mod. Phys.* **80**, 1455 (2008), [arXiv:0709.4635 \[hep-ph\]](#).
  - [6] B. Freedman and L. D. McLerran, *Phys. Rev. D* **17**, 1109 (1978).
  - [7] B. A. Freedman and L. D. McLerran, *Phys. Rev. D* **16**, 1169 (1977).
  - [8] E. Annala, T. Gorda, A. Kurkela, J. Nättilä, and A. Vuorinen, *Nature Phys.* **10.1038/s41567-020-0914-9** (2020), [arXiv:1903.09121 \[astro-ph.HE\]](#).
  - [9] T. Gorda, A. Kurkela, R. Paatelainen, S. Säppi, and A. Vuorinen, (2021), [arXiv:2103.07427 \[hep-ph\]](#).
  - [10] T. Gorda, A. Kurkela, R. Paatelainen, S. Säppi, and A. Vuorinen, (2021), [arXiv:2103.05658 \[hep-ph\]](#).
  - [11] E. S. Fraga, A. Kurkela, and A. Vuorinen, *Eur. Phys. J. A* **52**, 49 (2016), [arXiv:1508.05019 \[nucl-th\]](#).
  - [12] A. Kurkela, E. S. Fraga, J. Schaffner-Bielich, and A. Vuorinen, *Astrophys. J.* **789**, 127 (2014), [arXiv:1402.6618 \[astro-ph.HE\]](#).
  - [13] A. Kurkela, P. Romatschke, and A. Vuorinen, *Phys. Rev. D* **81**, 105021 (2010), [arXiv:0912.1856 \[hep-ph\]](#).
  - [14] Y. Fujimoto and K. Fukushima, (2020), [arXiv:2011.10891 \[hep-ph\]](#).
  - [15] H. Togashi, K. Nakazato, Y. Takehara, S. Yamamuro, H. Suzuki, and M. Takano, *Nucl. Phys. A* **961**, 78 (2017), [arXiv:1702.05324 \[nucl-th\]](#).
  - [16] A. Akmal, V. Pandharipande, and D. Ravenhall, *Phys. Rev. C* **58**, 1804 (1998), [arXiv:nucl-th/9804027](#).
  - [17] C. Drischler, K. Hebeler, and A. Schwenk, *Phys. Rev. Lett.* **122**, 042501 (2019), [arXiv:1710.08220 \[nucl-th\]](#).
  - [18] B. D. Carlsson, A. Ekström, C. Forssén, D. F. Strömberg, G. R. Jansen, O. Lilja, M. Lindby, B. A. Mattsson, and K. A. Wendt, *Phys. Rev. X* **6**, 011019 (2016), [arXiv:1506.02466 \[nucl-th\]](#).
  - [19] C. Drischler, K. Hebeler, and A. Schwenk, *Phys. Rev. C* **93**, 054314 (2016), [arXiv:1510.06728 \[nucl-th\]](#).
  - [20] J. E. Lynn, I. Tews, J. Carlson, S. Gandolfi, A. Gezerlis, K. E. Schmidt, and A. Schwenk, *Phys. Rev. Lett.* **116**, 062501 (2016), [arXiv:1509.03470 \[nucl-th\]](#).

- [21] J. Carlson, S. Gandolfi, F. Pederiva, S. C. Pieper, R. Schiavilla, K. E. Schmidt, and R. B. Wiringa, *Rev. Mod. Phys.* **87**, 1067 (2015), arXiv:1412.3081 [nucl-th].
- [22] M. Oertel, M. Hempel, T. Klähn, and S. Typel, *Rev. Mod. Phys.* **89**, 015007 (2017), arXiv:1610.03361 [astro-ph.HE].
- [23] Z. Arzoumanian *et al.* (NANOGrav), *Astrophys. J. Suppl.* **235**, 37 (2018), arXiv:1801.01837 [astro-ph.HE].
- [24] E. Fonseca *et al.*, *Astrophys. J.* **832**, 167 (2016), arXiv:1603.00545 [astro-ph.HE].
- [25] P. Demorest, T. Pennucci, S. Ransom, M. Roberts, and J. Hessels, *Nature* **467**, 1081 (2010), arXiv:1010.5788 [astro-ph.HE].
- [26] H. T. Cromartie *et al.*, *Nature Astron.* **4**, 72 (2019), arXiv:1904.06759 [astro-ph.HE].
- [27] E. Fonseca *et al.*, (2021), arXiv:2104.00880 [astro-ph.HE].
- [28] M. Miller *et al.*, *Astrophys. J. Lett.* **887**, L24 (2019), arXiv:1912.05705 [astro-ph.HE].
- [29] T. E. Riley *et al.*, *Astrophys. J. Lett.* **887**, L21 (2019), arXiv:1912.05702 [astro-ph.HE].
- [30] T. Kojo, *AAPPS Bull.* **31**, 11 (2021), arXiv:2011.10940 [nucl-th].
- [31] M. C. Miller *et al.*, (2021), arXiv:2105.06979 [astro-ph.HE].
- [32] T. E. Riley *et al.*, (2021), arXiv:2105.06980 [astro-ph.HE].
- [33] K. Masuda, T. Hatsuda, and T. Takatsuka, *Astrophys. J.* **764**, 12 (2013), arXiv:1205.3621 [nucl-th].
- [34] K. Masuda, T. Hatsuda, and T. Takatsuka, *PTEP* **2013**, 073D01 (2013), arXiv:1212.6803 [nucl-th].
- [35] K. Masuda, T. Hatsuda, and T. Takatsuka, *Eur. Phys. J. A* **52**, 65 (2016), arXiv:1508.04861 [nucl-th].
- [36] T. Kojo, P. D. Powell, Y. Song, and G. Baym, *Phys. Rev. D* **91**, 045003 (2015), arXiv:1412.1108 [hep-ph].
- [37] G. Baym, T. Hatsuda, T. Kojo, P. D. Powell, Y. Song, and T. Takatsuka, *Rept. Prog. Phys.* **81**, 056902 (2018), arXiv:1707.04966 [astro-ph.HE].
- [38] G. Baym, S. Furusawa, T. Hatsuda, T. Kojo, and H. Togashi, *Astrophys. J.* **885**, 42 (2019), arXiv:1903.08963 [astro-ph.HE].
- [39] Y.-L. Ma and M. Rho, *Prog. Part. Nucl. Phys.* **113**, 103791 (2020), arXiv:1909.05889 [nucl-th].
- [40] A. Ayriyan, D. Blaschke, A. G. Grunfeld, D. Alvarez-Castillo, H. Grigorian, and V. Abgaryan, (2021), arXiv:2102.13485 [astro-ph.HE].
- [41] P. Bedaque and A. W. Steiner, *Phys. Rev. Lett.* **114**, 031103 (2015), arXiv:1408.5116 [nucl-th].
- [42] I. Tews, J. Carlson, S. Gandolfi, and S. Reddy, *Astrophys. J.* **860**, 149 (2018), arXiv:1801.01923 [nucl-th].
- [43] C. Drischler, S. Han, J. M. Lattimer, M. Prakash, S. Reddy, and T. Zhao, (2020), arXiv:2009.06441 [nucl-th].
- [44] R. D. Pisarski, *Phys. Rev. D* **103**, L071504 (2021), arXiv:2101.05813 [nucl-th].
- [45] M. Hippert, E. S. Fraga, and J. Noronha, (2021), arXiv:2105.04535 [nucl-th].
- [46] A. Bazavov *et al.* (HotQCD), *Phys. Lett. B* **795**, 15 (2019), arXiv:1812.08235 [hep-lat].
- [47] L. McLerran and S. Reddy, *Phys. Rev. Lett.* **122**, 122701 (2019), arXiv:1811.12503 [nucl-th].
- [48] L. McLerran and R. D. Pisarski, *Nucl. Phys. A* **796**, 83 (2007), arXiv:0706.2191 [hep-ph].
- [49] L. Y. Glozman and R. F. Wagenbrunn, *Phys. Rev. D* **77**, 054027 (2008), arXiv:0709.3080 [hep-ph].
- [50] Y. Hidaka, L. D. McLerran, and R. D. Pisarski, *Nucl. Phys. A* **808**, 117 (2008), arXiv:0803.0279 [hep-ph].
- [51] L. McLerran, K. Redlich, and C. Sasaki, *Nucl. Phys. A* **824**, 86 (2009), arXiv:0812.3585 [hep-ph].
- [52] A. Andronic *et al.*, *Nucl. Phys. A* **837**, 65 (2010), arXiv:0911.4806 [hep-ph].
- [53] T. Kojo, Y. Hidaka, L. McLerran, and R. D. Pisarski, *Nucl. Phys. A* **843**, 37 (2010), arXiv:0912.3800 [hep-ph].
- [54] T. Kojo, R. D. Pisarski, and A. M. Tsvelik, *Phys. Rev. D* **82**, 074015 (2010), arXiv:1007.0248 [hep-ph].
- [55] T. Kojo, *Nucl. Phys. A* **877**, 70 (2012), arXiv:1106.2187 [hep-ph].
- [56] T. Kojo, Y. Hidaka, K. Fukushima, L. D. McLerran, and R. D. Pisarski, *Nucl. Phys. A* **875**, 94 (2012), arXiv:1107.2124 [hep-ph].
- [57] E. J. Ferrer, V. de la Incera, and A. Sanchez, *Acta Phys. Polon. Supp.* **5**, 679 (2012), arXiv:1205.4492 [nucl-th].
- [58] A. M. Tsvelik and R. D. Pisarski, (2021), arXiv:2103.15835 [nucl-th].
- [59] K. S. Jeong, L. McLerran, and S. Sen, *Phys. Rev. C* **101**, 035201 (2020), arXiv:1908.04799 [nucl-th].
- [60] D. C. Duarte, S. Hernandez-Ortiz, and K. S. Jeong, *Phys. Rev. C* **102**, 025203 (2020), arXiv:2003.02362 [nucl-th].
- [61] D. C. Duarte, S. Hernandez-Ortiz, and K. S. Jeong, *Phys. Rev. C* **102**, 065202 (2020), arXiv:2007.08098 [nucl-th].
- [62] S. Han, M. A. A. Mamun, S. Lalit, C. Constantinou, and M. Prakash, *Phys. Rev. D* **100**, 103022 (2019), arXiv:1906.04095 [astro-ph.HE].
- [63] T. Zhao and J. M. Lattimer, (2020), arXiv:2004.08293 [astro-ph.HE].
- [64] G. Cao and J. Liao, *JHEP* **10**, 168, arXiv:2007.02028 [nucl-th].
- [65] J. Margueron, H. Hansen, P. Proust, and G. Chanfray, (2021), arXiv:2103.10209 [nucl-th].
- [66] R. Somasundaram and J. Margueron, (2021), arXiv:2104.13612 [astro-ph.HE].
- [67] T. Kojo, *AIP Conf. Proc.* **2127**, 020023 (2019), arXiv:1904.05080 [astro-ph.HE].
- [68] D. Blaschke, M. Buballa, A. Dubinin, G. Roepke, and D. Zablocki, *Annals Phys.* **348**, 228 (2014), arXiv:1305.3907 [hep-ph].
- [69] T. Kojo, *Phys. Rev. D* **101**, 036001 (2020), arXiv:1811.07363 [hep-ph].
- [70] A. De Rujula, H. Georgi, and S. L. Glashow, *Phys. Rev. D* **12**, 147 (1975).
- [71] N. Isgur and G. Karl, *Phys. Rev. D* **20**, 1191 (1979).
- [72] M. Oka and K. Yazaki, *Phys. Lett. B* **90**, 41 (1980).
- [73] M. Oka and K. Yazaki, *Nucl. Phys. A* **402**, 477 (1983), [Erratum: *Nucl. Phys. A* 458, 773–773 (1986)].
- [74] A. Park, S. H. Lee, T. Inoue, and T. Hatsuda, *Eur. Phys. J. A* **56**, 93 (2020), arXiv:1907.06351 [hep-ph].
- [75] Y. Song, G. Baym, T. Hatsuda, and T. Kojo, *Phys. Rev. D* **100**, 034018 (2019), arXiv:1905.01005 [astro-ph.HE].
- [76] M. Leonhardt, M. Pospiech, B. Schallmo, J. Braun, C. Drischler, K. Hebeler, and A. Schwenk, *Phys. Rev. Lett.* **125**, 142502 (2020), arXiv:1907.05814 [nucl-th].
- [77] K. Fukushima, T. Kojo, and W. Weise, *Phys. Rev. D* **102**, 096017 (2020), arXiv:2008.08436 [hep-ph].
- [78] J. M. Luttinger and J. C. Ward, *Phys. Rev.* **118**, 1417 (1960).
- [79] G. Baym, *Phys. Rev.* **127**, 1391 (1962).

- [80] J. M. Cornwall, R. Jackiw, and E. Tomboulis, *Phys. Rev. D* **10**, 2428 (1974).
- [81] T. Kojo, *Eur. Phys. J. A* **52**, 51 (2016), [arXiv:1508.04408 \[hep-ph\]](#).
- [82] D. Suenaga and T. Kojo, *Phys. Rev. D* **100**, 076017 (2019), [arXiv:1905.08751 \[hep-ph\]](#).
- [83] T. Kojo, D. Hou, J. Okafor, and H. Togashi, (2020), [arXiv:2012.01650 \[astro-ph.HE\]](#).
- [84] T. Kojo and D. Suenaga, *Phys. Rev. D* **103**, 094008 (2021), [arXiv:2102.07231 \[hep-ph\]](#).
- [85] D. Suenaga and T. Kojo, (2021), [arXiv:2105.10538 \[hep-ph\]](#).